tvst

Article

Safety Profile of Slit-Lamp-Delivered Retinal Laser Photobiomodulation

Jack Ao[1], Glyn Chidlow[1], John P. M. Wood[1], and Robert J. Casson[1]

[1] Ophthalmic Research Laboratories, Discipline of Ophthalmology and Visual Sciences, University of Adelaide, Adelaide, South Australia, Australia

Correspondence: Robert J. Casson, Ophthalmic Research Laboratories, Discipline of Ophthalmology and Visual Sciences, University of Adelaide, Level 7 Adelaide Health and Medical Sciences Building, North Terrace, Adelaide, SA 5000, Australia. e-mail: robert.casson@adelaide.edu.au

Received: September 18, 2019
Accepted: January 10, 2020
Published: March 23, 2020

Keywords: photobiomodulation; retina; photoreceptors; laser; safety; gliosis

Citation: Ao J, Chidlow G, Wood JPM, Casson RJ. Safety profile of slit-lamp-delivered retinal laser photobiomodulation. Trans Vis Sci Tech. 2020;9(4):22, https://doi.org/10.1167/tvst.9.4.22

Purpose: Photobiomodulation (PBM) refers to therapeutic irradiation of tissue with low-energy, 630- to 1000-nm wavelength light. An increasing body of evidence supports a beneficial effect of PBM in retinal disorders. To date, most studies have utilized light-emitting diode irradiation sources. Slit-lamp-mounted retinal lasers produce a coherent beam that can be delivered with precisely defined dosages and predetermined target area; however, the use of retinal lasers raises safety concerns that warrant investigation prior to clinical application. In this study, we determined safe dosages of laser-delivered PBM to the retina.

Methods: A custom-designed, slit-lamp-delivered, 670-nm, red/near-infrared laser was used to administer a range of irradiances to healthy pigmented and non-pigmented rat retinas. The effects of PBM on various functional and structural parameters of the retina were evaluated utilizing a combination of electroretinography, Spectral Domain Optical Coherence (SD-OCT), fluorescein angiography, histology and immunohistochemistry.

Results: In non-pigmented rats, no adverse events were identified at any irradiances up to 500 mW/cm^2. In pigmented rats, no adverse events were identified at irradiances of 25 or 100 mW/cm^2; however, approximately one-third of rats that received 500 mW/cm^2 displayed very localized photoreceptor damage in the peripapillary region, typically adjacent to the optic nerve head.

Conclusions: A safety threshold exists for laser-delivered PBM in pigmented retinas and was identified as 500 mW/cm^2 irradiance; therefore, caution should be exercised in the dosage of laser-delivered PBM administered to pigmented retinas.

Translational Relevance: This study provides important data necessary for clinical translation of laser-delivered PBM for retinal diseases.

Introduction

The study of the therapeutic properties of light in the far-red and near-infrared range (630–1000 nm) began in the 1960s when it was serendipitously observed that the recently invented ruby laser enhanced wound healing in rats.[1] What was intended as a high-powered laser to destroy cancerous tissue inadvertently delivered low light energy, a form of phototherapy that is now known as photobiomodulation (PBM). Over the ensuing decades, the field of PBM has broadened to include treatment of a range of conditions, including chronic pain, muscle injury, and neurological dysfunction.[2] Although the exact mechanisms of action of PBM remain uncertain, robust evidence from absorption spectra indicates that a copper atom in Complex IV of the mitochondrial electron transport chain is the photoabsorber of PBM.[3] Correspondingly, PBM has been shown to promote electron transfer and redox activity.[4]

Among the variable-quality PBM literature are an increasing number of reports that have revealed positive effects of PBM delivered with light-emitting diodes (LEDs) to the retina. PBM has been shown to mitigate photoreceptor injury in a range of animal models, including methanol toxicity,[5] light-induced retinal damage,[6–12] and hyperoxia-induced degeneration in adults[13] and neonates.[14] PBM also mitigated pathophysiologic processes implicated in the patho-

genesis of diabetic retinopathy in mice[15] and reduced diabetic macular edema in a small case series of four patients.[16] These clinical findings were obtained using a commercially available red-light source that emits 670 nm light with a known irradiance at 1 inch from the device; however, the patients had their eyes closed during treatment (light passed through the eyelid) and the actual irradiance reaching the retina remains unknown. Furthermore, a recent interventional, longitudinal case series has found that LED-delivered PBM improved visual acuity and reduced drusen volume in patients with dry age-related macular degeneration.[17]

To date, the majority of studies investigating PBM have utilized LED irradiation sources.[18] LED-delivered PBM has been employed due to its safety, cost-effectiveness, ease of use, and ability to irradiate large areas. Although there remains controversy in the literature surrounding the merits of laser- versus LED-delivered PBM, laser-delivered PBM provides a familiar platform for clinicians. Slit-lamp-mounted retinal lasers produce a monochromatic, coherent beam of light that can be delivered by ophthalmologists with precisely defined dosages and a predetermined target area. In contrast, establishing therapeutic parameters for LED-delivered PBM is more problematic, as the radiation emitted is not coherent and hence is subject to scattering, absorption, and filtering by the structures of the eye. This rationale inspired us to develop a retinal PBM laser. Using this novel laser, we have recently produced exciting preliminary data showing a remarkable rescue of cones in a rodent model of retinitis pigmentosa,[19] and we have been granted approval for its use in patients with retinitis pigmentosa (Clinical Trial Registration no. ACTRN12618000651280p). However, the use of retinal laser raises safety concerns that warrant investigation before clinical employment. Herein, we report the first safety study of laser-delivered PBM to the retina. A custom-designed, slit-lamp delivered, 670-nm, red/near-infrared laser was used to administer a range of irradiances to healthy pigmented and non-pigmented rat retinas. Utilizing a combination of electroretinography, spectral-domain optical coherence tomography (SD-OCT), fluorescein angiography (FA), histology, and immunohistochemistry, the effects of PBM on various functional and structural parameters of the retina were evaluated.

Materials and Methods

Animals Ethics and Handling

This study was approved by the SA Pathology/Central Heath Network (CHN) Animal Ethics Committee (Adelaide, Australia) and conformed with the Australian Code of Practice for the Care and Use of Animals for Scientific Purposes (2013) and with the ARVO Statement for the Use of Animals in Vision and Ophthalmic Research. Adult Dark Agouti and Sprague–Dawley rats were housed in temperature- and humidity-regulated rooms with a 12-hour light/dark cycle and were provided with food and water ad libitum. For all procedures, rats received general anesthesia with an intraperitoneal injection of a mixture of 100 mg/kg ketamine and 10 mg/kg xylazine. At the conclusion of each experiment, animals were humanely killed by transcardial perfusion with physiological saline followed by neutral buffered formalin under terminal anesthesia.

Laser and PBM Procedure

The system is comprised of a custom-designed, slit-lamp-microscope-mounted Integre near-infrared laser (Ellex Medical Lasers, Adelaide, South Australia, Australia) incorporating a 670-nm light source emitting a beam 4.5 mm in diameter with a flat-top profile (Supplementary Fig. S1). Depending on the treatment group, the power setting was adjusted to produce the intended final irradiance at the retina (25–500 mW/cm^2). PBM was performed under isoflurane sedation, following topical instillation of 1% tropicamide to dilate the pupil and 0.5% amethocaine to provide corneal anesthesia. The animal was placed on a custom-designed platform attached to the slit lamp. The fundus was then imaged by placing a microscope coverslip lubricated with methylcellulose on the cornea. The power setting was adjusted to reflect the intended irradiance, and the laser was administered for 90 seconds by focusing and centering on the optic nerve head. This aiming approach was taken to optimize reproducibility, bearing in mind that the large spot size covered most of the rat retina.

Experiment 1: Safety in Pigmented Eyes Analyzed 1 Week Post-PBM

Initially, n = 4 eyes from each group (untreated control; sham, with aiming beam only; 25 mW/cm^2; 100 mW/cm^2; and 500 mW/cm^2) were treated. One of the 500-mW/cm^2 eyes displayed localized peripapillary changes; hence, further eyes were analyzed. In total, therefore, the number of eyes analyzed in each group was as follows: control (n = 6), sham (n = 7), 25 mW/cm^2 (n = 4), 100 mW/cm^2 (n = 7), and 500 mW/cm^2 (n = 10). Rats received three PBM treatments on non-consecutive days and were killed 1 week

after the final laser session (see Supplementary Fig. S2 for experimental plan and timeline). SD-OCT was performed on all rats at baseline and prior to killing. Concurrent with SD-OCT scans, fundus images were captured using a confocal scanning laser ophthalmoscope. Electroretinograms (ERGs) were conducted at baseline and at 7 days post-laser. While under terminal anesthesia, each rat underwent FA. Following euthanasia, globes with optic nerves attached were dissected for histological analysis.

Experiment 2: Safety in Pigmented Eyes Analyzed 3 Days Post-PBM

A follow-up experiment was performed in which rats were analyzed at an earlier time point to establish whether higher power PBM caused any overt vascular leakage or retinal edema in the first few days following multiple sessions of PBM. Rats received three PBM treatments on non-consecutive days and were killed 3 days after the final laser session. Fundus images were captured and SD-OCT performed on all rats at baseline and prior to killing. Each rat underwent FA prior to euthanasia. Following euthanasia, globes with optic nerves attached were dissected for histological analysis. The number of eyes analyzed in each group was as follows: sham (n = 3), 100 mW/cm^2 (n = 3), and 500 mW/cm^2 (n = 6).

Experiment 3: Safety in Non-Pigmented Eyes Analyzed 1 Week Post-PBM

A final experiment was performed using non-pigmented rats in order to reveal whether the peripapillary damage that was sometimes manifest at the high dose of PBM was conceivably related to absorption by the heavily pigmented retinal pigment epithelium (RPE)/choroid in the Dark Agouti strain. Rats received three PBM treatments on non-consecutive days and were killed 1 week after the final laser session. Fundus images were captured and SD-OCT performed on all rats at baseline and prior to killing. Each rat underwent FA prior to euthanasia. Following euthanasia, globes with optic nerves attached were dissected for histological analysis. The number of eyes analyzed in each group was as follows: sham (n = 3), 100 mW/cm^2 (n = 3), and 500 mW/cm^2 (n = 6).

Scotopic Electroretinography

Rats were dark-adapted overnight and maintained in dim red light. Electroretinography was performed under general anesthesia, following topical instillation of 1% tropicamide to dilate the pupil and 0.5% amethocaine to provide corneal anesthesia. The animal was placed on a heated platform to maintain body temperature throughout the procedure. Gold electrodes were used with the positive electrode placed on the central cornea and the reference electrode on the tongue, and the ground electrode was attached to the scruff of the neck. Preservative-free lubricating eye drops were applied to prevent exposure keratopathy. The flash stimulus was delivered from a custom-designed mini-Ganzfeld photic stimulator (20 cd·s/m^2, 0.1 Hz). The signals were amplified (gain set at 1000) and filtered (0.3-Hz high pass to 300-Hz low pass) with a DC amplifier (ADInstruments, New South Wales, Australia). All recordings were performed in complete darkness. Ten responses were recorded and averaged with LabChart software (ADInstruments). The amplitude and implicit times of the a- and b-waves were measured.

Spectral Domain Optical Coherence Tomography

SD-OCT was performed under general anesthesia following topical instillation of 1% tropicamide to dilate the pupil and 0.5% amethocaine to provide corneal anesthesia. Rats were placed on a custom-designed platform. SD-OCT was performed using the Heidelberg Spectralis (Heidelberg Engineering, Heidelberg, Germany). A wide-field 55° lens was used to capture an overall view of the retina. A series of 97 B-scan SD-OCT images were then taken at the optic nerve head (ONH), an area entirely contained within the lased area and measuring 2.4 × 1.7 mm. The distance between each B-scan was 18 µm. A confocal scanning laser ophthalmoscopy image of the corresponding fundus was also taken. The corneal curvature was adjusted to 3.0 mm, appropriate for rats, to allow accurate scaling for subsequent thickness measurements.[20] Throughout the procedure, preservative-free lubricant eye drops were administered to the eye to prevent corneal dryness and image artifacts. The total retinal thickness and outer nuclear layer (ONL) thickness were measured at specified points using the built-in Heidelberg Spectralis software (see Supplementary Fig. S3 for details). Thickness measurements were averaged for each eye.

Fluorescein Angiography

FA was performed under general anesthesia following topical instillation of 1% tropicamide to dilate the pupil. Sodium fluorescein (10%, w/v) 5 mL was injected intraperitoneally. Rats were placed on

a custom-designed platform. FA images were taken with the Heidelberg Spectralis in Angiography mode. Images of the retinal vessels were captured at 0, 5, 10, 15, and 20 minutes after fluorescein injection. Preservative-free lubricant eye drops were administered to prevent corneal dryness and image artifacts throughout the scanning process. Images were analyzed for any leakage, which was defined as any focal hyperfluorescence that increased in intensity and size over time.

Histology and Immunohistochemistry

Prior to enucleation, the superior aspect of each globe was marked using surgical ink for the purpose of orientation. Globes and optic nerves were carefully removed and immersion-fixed in 10% buffered formalin for at least 24 hours. Tissues were then processed for routine paraffin-embedded sections, with globes embedded sagittally and optic nerves longitudinally, and 4-µm sections were cut. Tissue sections were stained for hematoxylin and eosin using a standard methodology. Colorimetric immunohistochemistry was performed as previously described.[21,22] In brief, tissue sections were de-paraffinized, endogenous peroxidase activity was blocked, and high-temperature antigen retrieval was performed. Subsequently, sections were incubated in primary antibody (Supplementary Table S1), followed by consecutive incubations with biotinylated secondary antibody and streptavidin–peroxidase conjugate. Color development was achieved using 3,3′-diaminobenzidine.

Evaluation of Immunohistochemistry

All analyses were conducted in a blinded fashion. Photomicrographs of labeled tissue sections were taken under a light microscope (BX-51; Olympus Australia, Mount Waverly, Victoria, Australia).

Retina

From each labeled section, rectangular areas of 350 × 260 µm were photographed adjacent to the optic nerve head on each side and 1 mm away from the optic nerve head on each side. For quantification of glial fibrillary acidic protein (GFAP), ionized calcium binding adaptor molecule 1 (iba1), fibroblast growth factor 2 (FGF2), and ciliary neurotrophic factor (CNTF), the immunoreactive area in each photomicrograph was demarcated. First, color deconvolution was applied to extract the 3,3′-diaminobenzidine staining. Any uneven illuminated background was removed using the "rolling ball" method. After manual thresholding, the area of positive staining was then measured. Evaluations were performed using ImageJ 1.42q software (National Institutes of Health, Bethesda, MD, USA; http://rsb.info.nih.gov/ij/). For retinal ganglion cell (RGC) survival, all analyses were performed on sections taken at the level of the optic nerve head. The number of Brn3a-positive cells was quantified for a distance of 2 mm either side of the optic nerve head, approximately equating to the area of irradiance.

Optic Nerve

Axonal injury was quantitatively assessed by immunolabeling for SMI-32, an antibody that recognizes the non-phosphorylated neurofilament heavy chain. SMI-32 has been consistently demonstrated to be a highly sensitive, marker of axonal cytoskeleton disruption.[23] Quantification of immunolabeling was performed as previously described.[23]

Statistical Analysis

All data are presented as mean ± SEM. ERG and SD-OCT measurements were analyzed using Student's paired *t*-test for each treatment group (baseline vs. post-PBM). Immunohistochemistry for GFAP, iba1, FGF2, and CNT were analyzed by analysis of variance (ANOVA). Statistical analysis and generation of graphs were performed using GraphPad Prism 6 software (GraphPad Software, La Jolla, CA, USA). $P < 0.05$ was considered statistically significant.

Results

Safety Study in Pigmented Rats Analyzed 1 Week Post-PBM

Fundus Imaging

Qualitative assessment revealed that none of the eyes from the control, sham, 25 mW/cm^2, or 100 mW/cm^2 groups displayed any abnormalities on fundus imaging (for representative images, see Fig. 1). This was not the case for the 500 mW/cm^2 group. Six of 10 eyes treated with 500 mW/cm^2 PBM were normal; however, the remaining four eyes had noticeable fundus changes (Fig. 1, Supplementary Fig. S4). Evaluation of the fundus images of all four affected rats identified pigment changes bordering the ONH. The size of the affected area varied among rats, but it was always peripapillary and thus situated close to the epicenter of the irradiated area.

Spectral-Domain Optical Coherence Tomography

Imaging of every eye from the control, sham, 25 mW/cm^2, and 100 mW/cm^2 groups revealed an

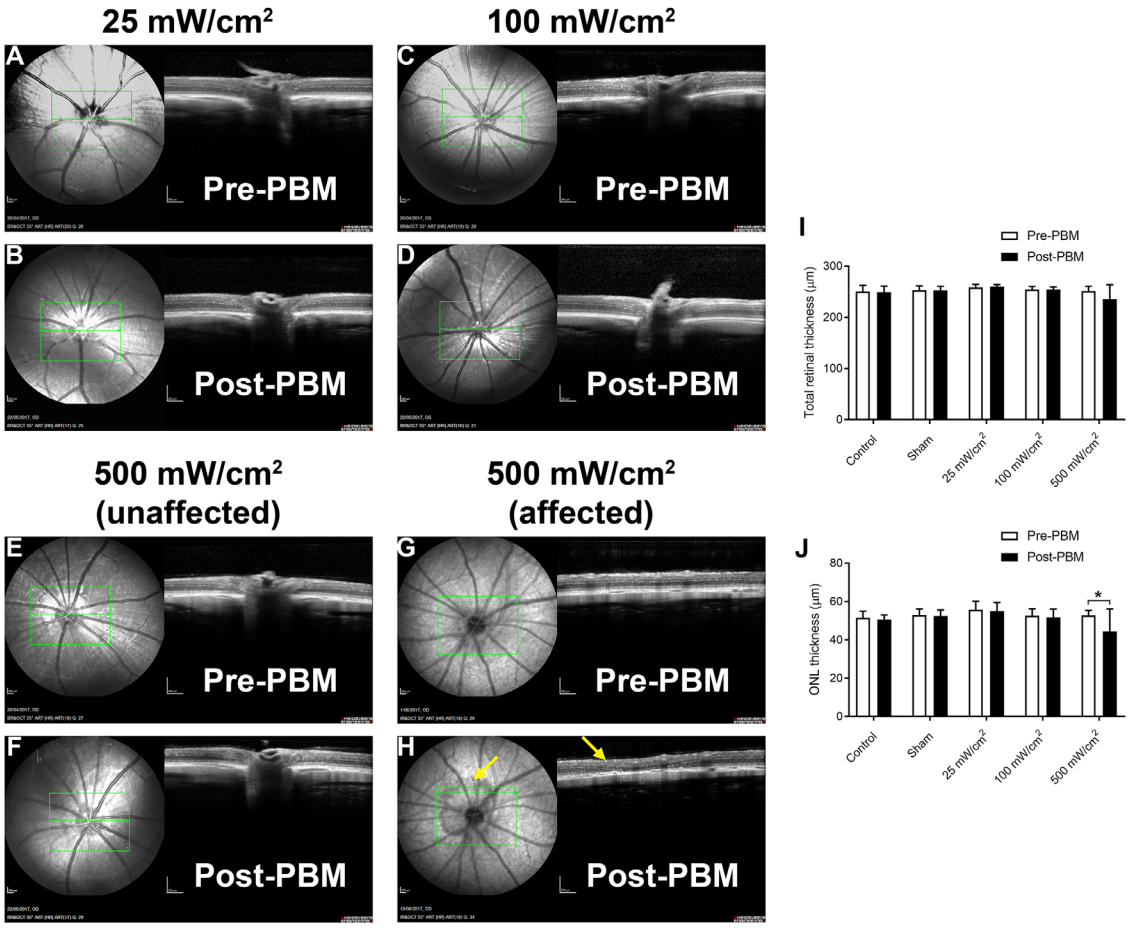

Figure 1. Effect of PBM on retinal integrity in pigmented rats at 1 week after the final treatment, as evaluated by fundus imaging and SD-OCT. Pre-treatment and post-treatment fundus and SD-OCT images of representative rats from 25 mW/cm^2 (A, B), 100 mW/cm^2 (C, D), and 500 mW/cm^2 (E–H) treatment groups are shown. Two different eyes from the 500 mW/cm^2 treatment group are highlighted: an "unaffected" eye (E, F) and an "affected" eye (G, H). In the 25 mW/cm^2, 100 mW/cm^2, and 500 mW/cm^2 unaffected eyes, there are no readily discernible abnormalities in either the fundus image or SD-OCT between baseline and post-PBM. In the 500 mW/cm^2 affected eye, there is a marked pigment change around the optic nerve head on fundus imaging (H, arrow) and localized damage to the ONL, which appears thinned and disorganized, by SD-OCT (H, arrow). Quantification of total retinal thickness (I) and ONL thickness (J), as defined in the Materials and Methods section, is provided. Data are expressed as the mean ± SEM, where n = 4–10 for each group. $^*P < 0.05$ by Student's paired *t*-test (pre-PBM vs. post-PBM).

unchanged profile relative to baseline (for representative images, see Fig. 1). Accordingly, paired Student's *t*-test analysis showed no significant difference in total retinal thickness or ONL thickness (baseline vs. post-PBM) in each of the groups (Fig. 1). Six of the 10 eyes treated with 500 mW/cm^2 PBM (those that featured a normal fundus) likewise appeared normal on SD-OCT (Fig. 1). The remaining four eyes treated with 500 mW/cm^2 PBM (those that featured fundus changes) also displayed abnormalities on SD-OCT, which were principally evident as localized damage to the ONL (Fig. 1). The mean total retinal thickness of the 500 mW/cm^2 group as a whole was 15.6 ± 6.9 µm thinner than baseline, a difference that almost reached significance ($P = 0.051$), and the ONL thickness was 8.4 ± 3.7 µm thinner than baseline, a value that was statistically significant ($P < 0.05$). The explanation for the small reductions in total retinal thickness and ONL thickness is that only four of 10 eyes were affected, coupled with the fact that 12 measurements were taken for each parameter per eye encompassing an area of 1 mm^2. Because the affected area of damage was quite localized, the majority of readings were normal.

Fluorescein Angiograms

Fluorescein angiograms taken of every eye from the control, sham, 25 mW/cm^2, and 100 mW/cm^2 groups showed normal vasculature and no fluorescein leakage (for representative images, see Fig. 2). Eight of 10 eyes treated with 500 mW/cm^2 PBM were normal (Fig. 2);

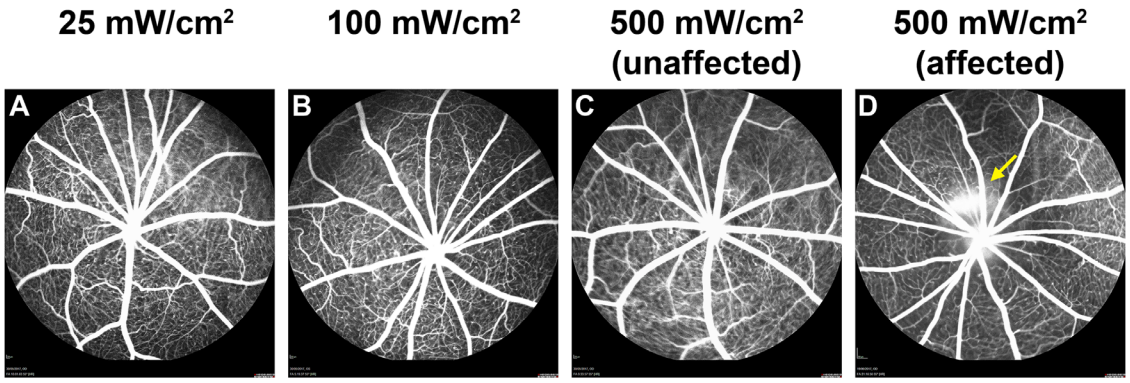

Figure 2. Effect of PBM on retinal integrity in pigmented rats at 1 week after the final treatment, as evaluated by fluorescein angiography. Post-treatment images of representative rats from 25 mW/cm^2 (A), 100 mW/cm^2 (B), and 500 mW/cm^2 (C, D) treatment groups are shown. Two different eyes from the 500 mW/cm^2 treatment group are highlighted: an "unaffected" eye (C) and an "affected" eye (D). Images were captured 15 to 20 minutes after injection of sodium fluorescein. In the 25 mW/cm^2, 100 mW/cm^2, and 500 mW/cm^2 unaffected eyes, there is no evidence of fluorescein leakage. In the 500 mW/cm^2 affected eye, there is very localized fluorescein leakage, apparent as cloudy hyperfluorescence, superior to the optic nerve head (arrow).

Table 1. Effect of PBM on b-Wave Amplitude Analyzed 1 Week Post-PBM

Treatment Group	Baseline b-Wave Amplitude (μv)	Post-PBM b-Wave Amplitude (μv)	Difference b-Wave Amplitude (μv)	*P*
Control	837.5 ± 92.5	868.8 ± 54.0	31.3 ± 38.9	0.54
Sham	907.1 ± 42.2	917.9 ± 29.8	10.7 ± 47.3	0.84
25 mW/cm^2	825.0 ± 85.4	823.8 ± 51.5	−1.2 ± 53.2	0.98
100 mW/cm^2	903.6 ± 32.9	900.0 ± 39.3	−3.6 ± 43.6	0.94
500 mW/cm^2	941.0 ± 41.4	935.0 ± 33.4	−6.0 ± 33.7	0.86

Data are expressed as mean ± SEM, where n = 6 (control), n = 7 (sham), n = 4 (25 mW/cm^2), n = 7 (100 mW/cm^2), and n = 10 (500 mW/cm^2).

however, two of 10 eyes treated with 500 mW/cm^2 PBM displayed abnormal fluorescein leakage (Fig. 2, Supplementary Fig. S4) that was present immediately upon injection of fluorescein, reached a peak after 15 minutes, and plateaued until 20 minutes before subsiding. The affected eyes were from the subcohort that also showed fundus and SD-OCT changes. The leakage most likely derives from deep within the retina, either at the deep capillary plexus or from the choroid. There were no other morphological vascular abnormalities.

Electroretinograms

The ERGs remained unaffected by multiple PBM sessions, irrespective of the energy setting. Representative baseline and post-PBM ERG traces in the different treatment groups are shown in Supplementary Fig. S5, and the b-wave and a-wave amplitudes in each group are provided in Tables 1 and 2, respectively; the b-wave and a-wave implicit times are documented in Supplementary Tables S2 and S3, respectively. Paired Student's *t*-test analysis revealed no statistical difference in a-wave or b-wave amplitudes in any of the treatment groups (baseline vs. post-PBM). Similarly, a-wave and b-wave implicit times were also not significantly altered in any of the treatment groups (baseline vs. post-PBM). Because fundus changes and localized retinal damage were evident in four of 10 rats from the highest energy setting (500 mW/cm^2; see below), we analyzed this subgroup of affected rats independently. The data showed that, in affected eyes from the 500 mW/cm^2 group, there was no significant difference in the amplitudes of the b-wave (900 ± 84 μV at baseline vs. 937 ± 47 μV post-PBM) or a-wave (225 ± 62 μV at baseline vs. 213 ± 31 μV post-PBM).

Histology

Gross examination of whole eyes analyzed 1 week post-PBM showed no retinal hemorrhages or cataracts in eyes from any of the treatment groups. Histological evaluation of the ONH and retina from control,

Table 2. Effect of PBM on a-Wave Amplitude Analyzed 1 Week Post-PBM

Treatment Group	Baseline a-Wave Amplitude (μV)	Post-PBM a-Wave Amplitude (μV)	Difference a-Wave Amplitude (μV)	*P*
Control	200.0 ± 45.9	225.0 ± 28.0	25.0 ± 23.4	0.42
Sham	225.0 ± 21.1	203.6 ± 11.8	−21.4 ± 23.4	0.43
25 mW/cm^2	137.5 ± 23.9	156.3 ± 21.3	18.8 ± 31.3	0.59
100 mW/cm^2	196.4 ± 20.7	203.6 ± 15.8	7.1 ± 26.6	0.81
500 mW/cm^2	230.0 ± 24.1	207.5 ± 12.9	−22.5 ± 15.1	0.17

Data are expressed as mean ± SEM, where n = 6 (control), n = 7 (sham), n = 4 (25 mW/cm^2), n = 7 (100 mW/cm^2), and n = 10 (500 mW/cm^2).

sham, 25 mW/cm^2, and 100 mW/cm^2 groups yielded results that were entirely consistent with those obtained from fundus imaging, SD-OCT, and FA. Specifically, there was no evidence of photoreceptor damage, disorganization of photoreceptor segments, macro- or microgliosis, upregulation of stress proteins, or damage to the RPE, either within the peripapillary zone or throughout the remainder of the irradiated zone (Figs. 3, 4). There was also no indication of any disorganization of the inner retina.

Examination of rats treated with 500 mW/cm^2 confirmed and extended the findings obtained from fundus imaging and SD-OCT. Thus, in six of 10 eyes (those that appeared normal on fundus imaging and SD-OCT) there was no evidence of inner or outer retinal damage, macro- or microgliosis, or injury to the RPE, either within the peripapillary zone or throughout the remainder of the irradiated zone (Fig. 4). However, the remaining four eyes treated with 500 mW/cm^2 PBM (those that featured fundus and SD-OCT abnormalities) displayed very localized histological damage adjacent to the ONH (for the worst affected eye, see Fig. 3). The affected retinal regions in these rats were markedly disorganized and featured loss of photoreceptor nuclei, as well as inner and outer segments. This was accompanied by localized upregulations of the stereotypical macroglial stress markers GFAP and CNTF. Furthermore, an increased microglial presence was evident in the affected region, particularly in the degenerating outer nuclear layer. The RPE layer was mostly intact in the affected peripapillary zone, but individual areas of thinning and damage, or hypertrophy indicative of cell death and subsequent regeneration, could be discerned. The inner retina, overlying the disturbed photoreceptors, of affected rats remained structurally intact. Aside from the localized area of damage, minimal injury or glial responses could be observed in other areas around the ONH in the four affected rats, data in agreement with the fundus images. Similarly, no injury was manifest in the remainder of the irradiated zone (Fig. 4). Quantification of the retinal levels of GFAP, iba1, CNTF, and FGF2 in photomicrographs taken 1 mm away from the ONH in either direction (locations within the 4.5-mm beam) showed no upregulation of any of these markers in the 500 mW/cm^2 group relative to the control group ($P = 0.24$, $P = 0.21$, $P = 0.95$, and $P = 0.61$, respectively, by unpaired Student's *t*-test).

Mitochondria are highly enriched in RGCs, particularly within their unmyelinated axons that form the nerve fiber layer. As such, it was important to ascertain whether laser-delivered PBM causes any damage to this important class of neurons. Quantification of the number of RGCs in retinal tissue sections revealed no difference among the various treatment groups (Supplementary Figs. S6A–S6D). Likewise, immunolabeling optic nerve tissue sections with an antibody directed against the non-phosphorylated chain of neurofilament heavy, a sensitive marker of axonal breakdown, showed no disturbance to the integrity of the axonal cytoskeleton at any of the energy settings tested (Supplementary Figs. S6E–S6J).

Safety Study in Pigmented Rats Analyzed 3 Days Post-PBM

The overall data demonstrate that low to moderate power settings of the retinal PBM laser are safe in pigmented rodents, but the highest power setting tested (500 mW/cm^2) has the capacity to cause localized peripapillary injury, which was characterized by pigmentary changes to the fundus, outer retinal damage, and sometimes vascular leakage. A follow-up experiment was performed in which rats were analyzed at an earlier time point, 3 days post-PBM, in order to establish whether any overt vascular leakage or retinal edema occurred in the first few days following multiple sessions of PBM that may have been underestimated when rats were analyzed one week following the final PBM session. Because no changes to retinal function,

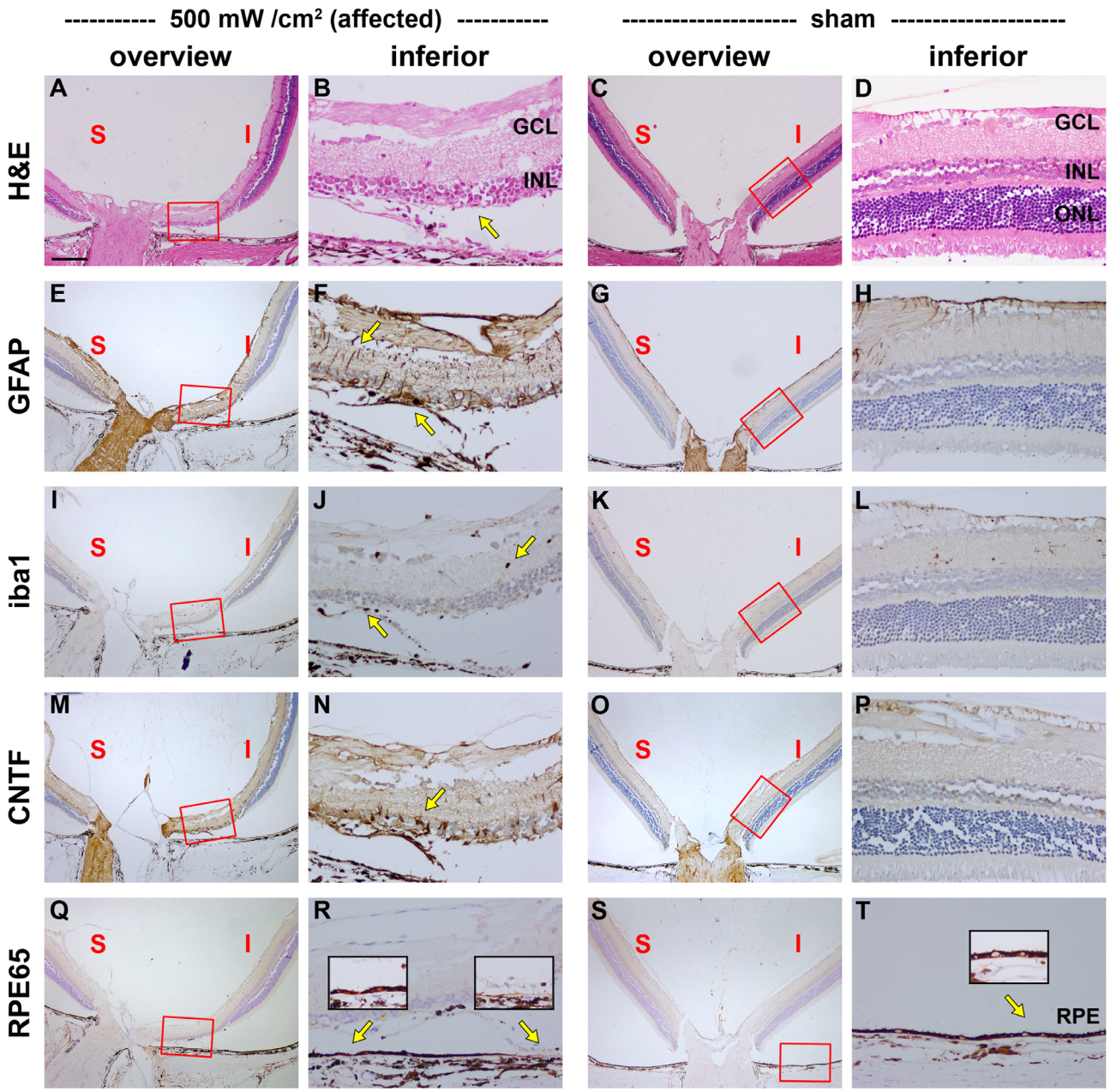

Figure 3. Effect of PBM on ONH integrity in pigmented rats at 1 week after the final treatment, as evaluated by histology and immunohistochemistry. Histology of an affected rat from the 500 mW/cm^2 group and a representative rat from the sham group are shown. Transverse sections at the level of the ONH were stained for hematoxylin and eosin (A–D) and immunolabeled for GFAP (E–H), iba1 (I–L), CNTF (M–P), and RPE65 (Q–T). In the affected rat from the 500 mW/cm^2 group, there is localized destruction of photoreceptor nuclei and inner and outer segments immediately inferior to the ONH (A, B, arrow). This is accompanied by greatly increased expression of GFAP (E, F, arrows) and CNTF (M, N, arrows) by Müller cells and astrocytes overlying and immediately adjacent to the affected area. Iba1-positive activated microglia can be observed within the damaged area of the retina (I, J, arrows). The RPE layer appears relatively intact, but discrete areas of injury are apparent (Q, R, arrows, highlighted within insets). On the superior side of the ONH, there is no patent injury or upregulation of glial markers. In the sham rat, there is no evidence of any abnormalities in any of the markers analyzed. *Scale bar*: 250 µm (A, C, E, G, I, K, M, O, Q, S). *Scale bar*: 50 µm (B, D, F, H, J, L, N, P, R, T). GCL, ganglion cell layer; INL, inner nuclear layer.

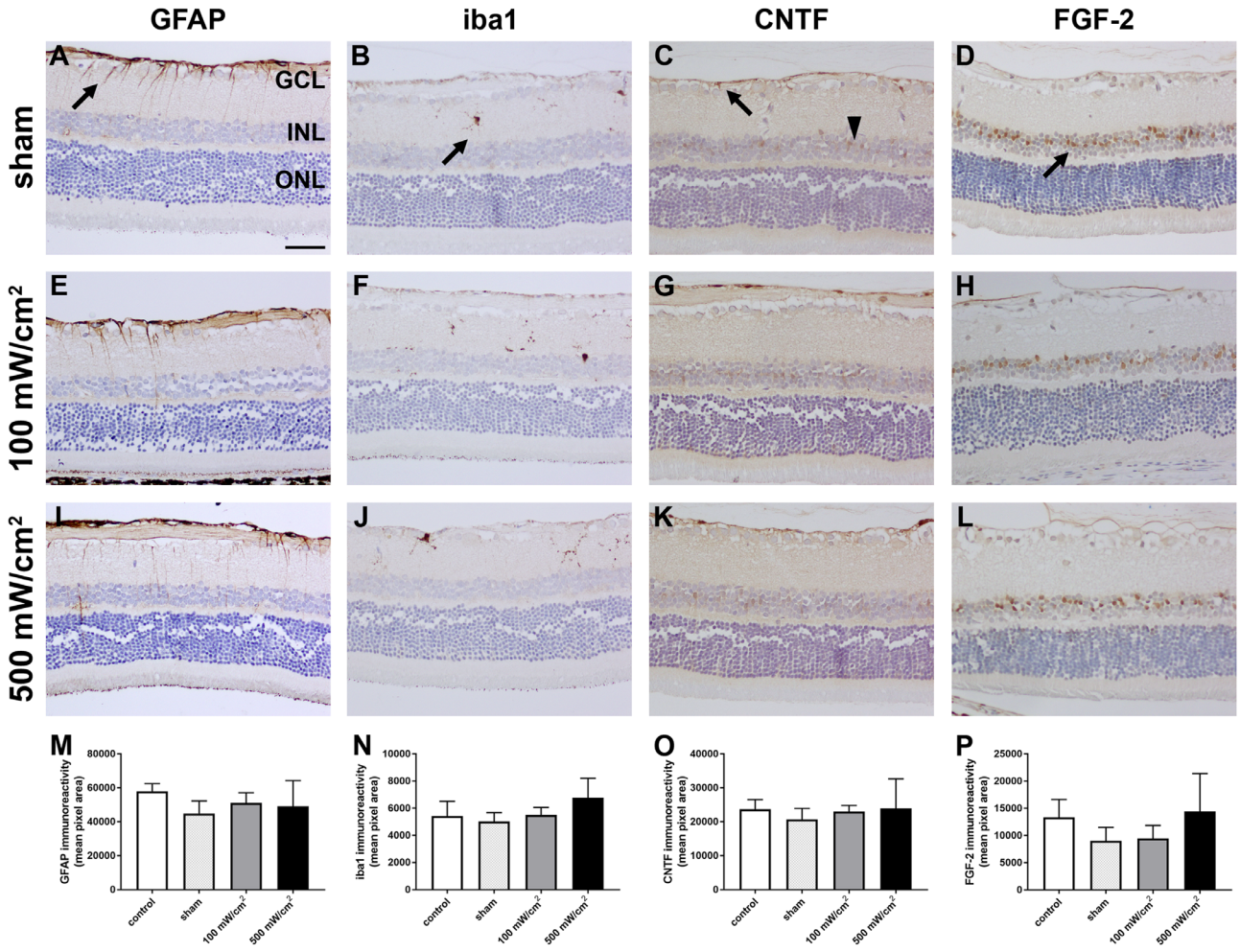

Figure 4. Effect of PBM on glial markers and stress proteins in the retina in pigmented rats at 1 week after the final treatment, as evaluated by immunohistochemistry. Representative images of retinas from sham, 100 mW/cm^2, and 500 mW/cm^2 groups immunolabeled for GFAP (A, E, I), Iba1 (B, F, J), CTNF (C, G, K), and FGF2 (D, H, L) are shown. Images were captured within the irradiated zone at approximately 1 mm from the optic nerve head. In sham rats, GFAP is principally expressed by astrocytes and Müller cell endfeet (A, arrow), and there is a relatively sparse population of ramified iba1-positive microglia within the inner retina (B, arrow). In sham rats, astrocytes (C, arrow) and Müller cell somas (C, arrowhead) are weakly positive for CNTF, and Müller cell somas are positive for FGF2 (D, arrow). No discernible upregulation of any of the four markers is evident in rats treated with PBM (E–L). Quantification of GFAP (M), iba1 (N), CNTF (O), and FGF2 (P) abundances, as defined in the Materials and Methods section, are provided. Data are expressed as the mean ± SEM, where n = 6–10 for each group. ANOVA revealed no significant differences in abundances of GFAP, iba1, CNTF, or FGF2 among treatment groups. *Scale bar*: 50 µm. GCL, ganglion cell layer; INL, inner nuclear layer.

as assessed by pan-retinal scotopic ERG, were manifest in affected rats, ERG was not conducted in this follow-up study.

Fundus Imaging

Qualitative assessment revealed that none of the eyes from the sham or 100 mW/cm^2 groups displayed any abnormalities on fundus imaging (data not shown). Of the 500 mW/cm^2 group, four of six eyes treated were normal (Fig. 5); however, the remaining two eyes had fundus changes (Fig. 5, Supplementary Fig. S7). Evaluation of the fundus images of the affected rats identified changes comparable to those at the 1-week time point—namely, pigmentary changes in a small area bordering the ONH.

Spectral-Domain Optical Coherence Tomography

Imaging of eyes from the sham and 100 mW/cm^2 groups revealed an unchanged profile relative to baseline (data not shown). Accordingly, paired Student's *t*-test analysis showed no significant difference in total retinal thickness or ONL thickness (baseline vs. post-PBM) in either of the groups (Fig. 5). Four of the six eyes treated with 500 mW/cm^2

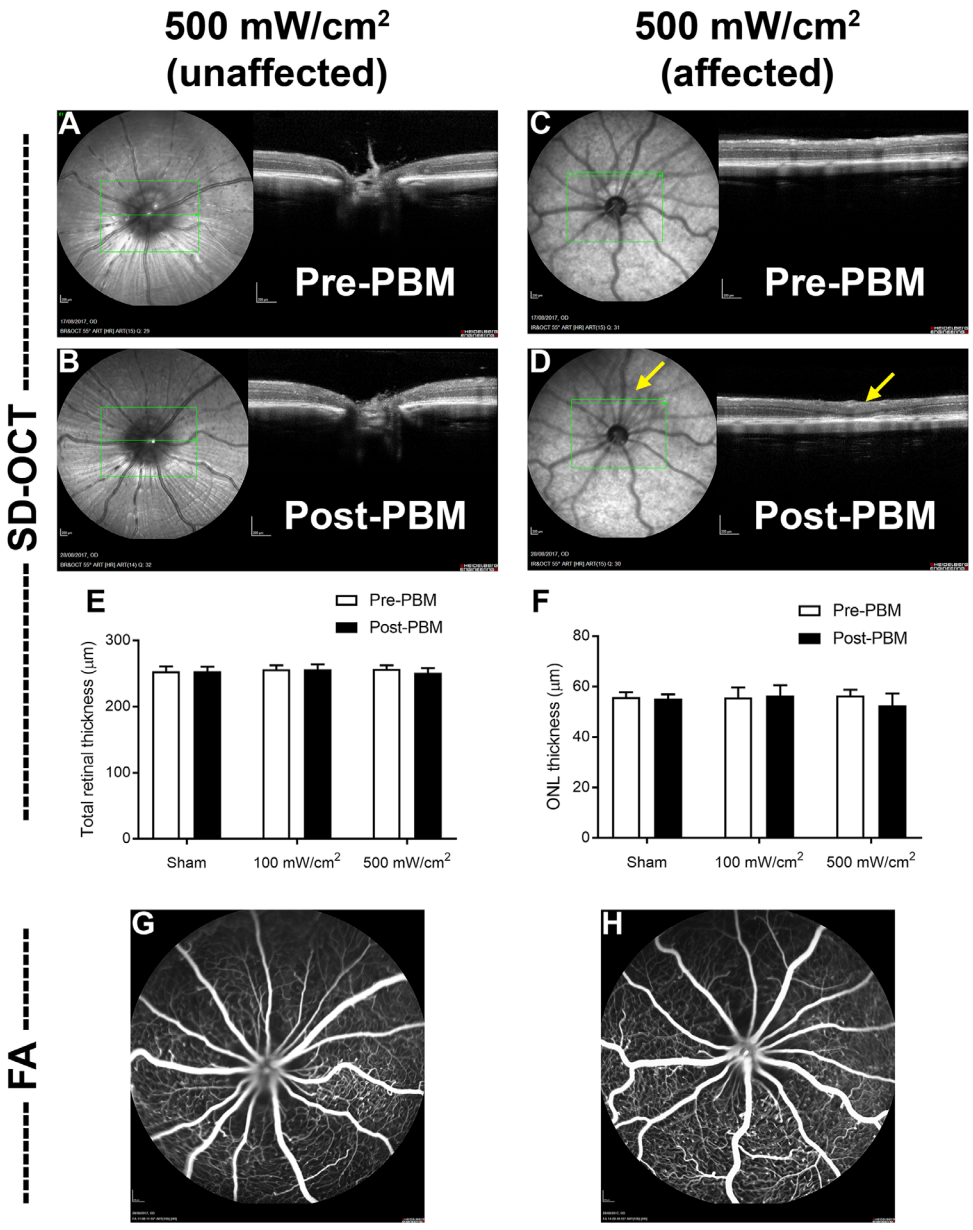

Figure 5. Effect of PBM on retinal integrity in pigmented rats at 3 days after the final treatment, as evaluated by fundus imaging, SD-OCT, and FA. Pre-treatment and post-treatment fundus and SD-OCT images of representative rats from the 500 mW/cm^2 treatment group are shown (A–D). Two different eyes are highlighted: an "unaffected" eye and an "affected" eye. In the 500 mW/cm^2 unaffected eye, there is no readily discernible abnormalities in either the fundus image or SD-OCT between baseline and post-PBM (A, B). In the 500 mW/cm^2 affected eye (C, D), there is a marked pigment change around the optic nerve head on fundus imaging (C, arrow) and localized damage to the outer nuclear layer, which appears thinned and disorganized, by SD-OCT (C, arrow). Quantification of total retinal thickness (E) and ONL thickness (F) in the different treatment groups, as defined in the Materials and Methods section, is provided. Data are expressed as the mean ± SEM, where n = 3–6 for each group. Corresponding post-treatment FA images are shown (G, H). Images were captured 15 to 20 minutes after injection of sodium fluorescein. Images of both eyes appear normal.

PBM (those that featured a normal fundus) likewise appeared normal on SD-OCT (Fig. 5). The remaining two eyes treated with 500 mW/cm^2 PBM (those that featured fundus changes) also displayed abnormalities on SD-OCT, which again were primarily evident as localized damage to the ONL (Fig. 5). The mean total retinal thickness of the 500 mW/cm^2 group as a whole was 5.7 ± 3.3 μm thinner than baseline, whereas the ONL thickness was 3.9 ± 2.8 μm thinner than baseline. Neither of these values approached significance

($P = 0.15$ and $P = 0.22$, respectively). As for the 1-week study, the small reductions in total retinal thickness and ONL thickness reflected the nature of the study design.

Fluorescein Angiograms

Angiograms taken from every eye from the sham, 100 mW/cm^2, and 500 mW/cm^2 groups showed normal vasculature and no fluorescein leakage at 3 days post-laser, including the two affected eyes from the 500 mW/cm^2 group that had peripapillary abnormalities as evidenced by fundus imaging, SD-OCT, and histology (Fig. 5, Supplementary Fig. S7).

Histology

Gross examination of whole eyes analyzed 3 days post-PBM showed no retinal hemorrhages or cataracts in any eyes. Histological evaluation of the ONH and retina from the sham and 100 mW/cm^2 groups yielded results that were consistent with those obtained from fundus imaging and SD-OCT. Specifically, there was no evidence of abnormalities in the inner or outer retina, macro- or microgliosis, upregulation of stress proteins, or damage to the RPE, either within the peripapillary zone or throughout the remainder of the irradiated zone (Figs. 6, 7).

Histological examination of rats treated with 500 mW/cm^2 confirmed and extended the findings obtained from fundus imaging and SD-OCT. Thus, in four of six eyes (those that appeared normal on fundus imaging and SD-OCT), there was no evidence of inner or outer retinal damage, macro- or microgliosis, or injury to the RPE, either within the peripapillary zone or throughout the remainder of the irradiated zone (Fig. 7). However, the remaining two eyes treated with 500 mW/cm^2 PBM (those that featured fundus and SD-OCT changes) displayed very localized histological damage adjacent to the ONH (Fig. 6). The affected rats featured localized retinal disorganization including loss of rod and cone nuclei as well as inner and outer segments. This was accompanied by localized upregulation of GFAP and CNTF. Furthermore, a dramatically increased microglial presence was evident in the affected region, particularly in the degenerating outer nuclear layer. Overt damage to the RPE layer could also be discerned. The inner retina of affected rats remained structurally intact. Unlike the 1-week experiment, subtle retinal stress responses, such as upregulation of GFAP and FGF2, could be observed in occasional eyes 1 mm from the ONH on the affected side, a distance well within the irradiated zone (Fig. 7). Nevertheless, quantification of the levels of GFAP, iba1, CNTF, and FGF2 showed no statistically significant upregulation of any of these markers in the 500 mW/cm^2 group relative to the other groups ($P = 0.48$ vs. $P = 0.72$, $P = 0.97$, and $P = 0.55$, respectively, by ANOVA) (Fig. 7). Quantification of the number of RGCs in retinal tissue sections and the number of axonal cytoskeletal abnormalities in the optic nerve sections revealed no evidence of any toxicity in the PBM groups (data not shown).

Safety Study in Non-Pigmented Rats Analyzed 1 Week Post-PBM

A final experiment was performed using a non-pigmented rat strain in order to reveal whether the peripapillary damage that was sometimes manifest following multiple sessions of 500 mW/cm^2 PBM in pigmented rats might be related to absorption by the heavily pigmented RPE/choroid.

Fundus Imaging

Qualitative assessment revealed that none of the eyes from the sham, 100 mW/cm^2, or 500 mW/cm^2 groups displayed any abnormalities on fundus imaging (Fig. 8). Unlike in pigmented rats, the highest energy setting caused no focal damage noted within the peripapillary zone in any of the six non-pigmented eyes analyzed.

Spectral-Domain Optical Coherence Tomography

Imaging of eyes from all three groups revealed unchanged profiles relative to baseline (Fig. 8). Accordingly, paired Student's *t*-test analysis showed no significant difference in total retinal thickness or ONL thickness (baseline vs. post-PBM) in any of the treatment groups (Fig. 8).

Fluorescein Angiograms

Angiograms taken of every eye from the sham, 100 mW/cm^2, and 500 mW/cm^2 groups showed normal vasculature and no fluorescein leakage at 1 week post-laser (Fig. 8).

Histology

Gross examination of whole eyes analyzed 1 week post-PBM showed no retinal hemorrhages or cataracts in any eyes. Histological evaluation of the ONH and retina from all three groups yielded results that were consistent with those obtained from fundus imaging and SD-OCT. Specifically, there was no evidence of photoreceptor injury, macro- or microgliosis, upregulation of stress proteins, or damage to the RPE, either within the peripapillary zone (for representative histology of the 500 mW/cm^2-treated Sprague–Dawley rat, see Fig. 9) or throughout the remainder of the

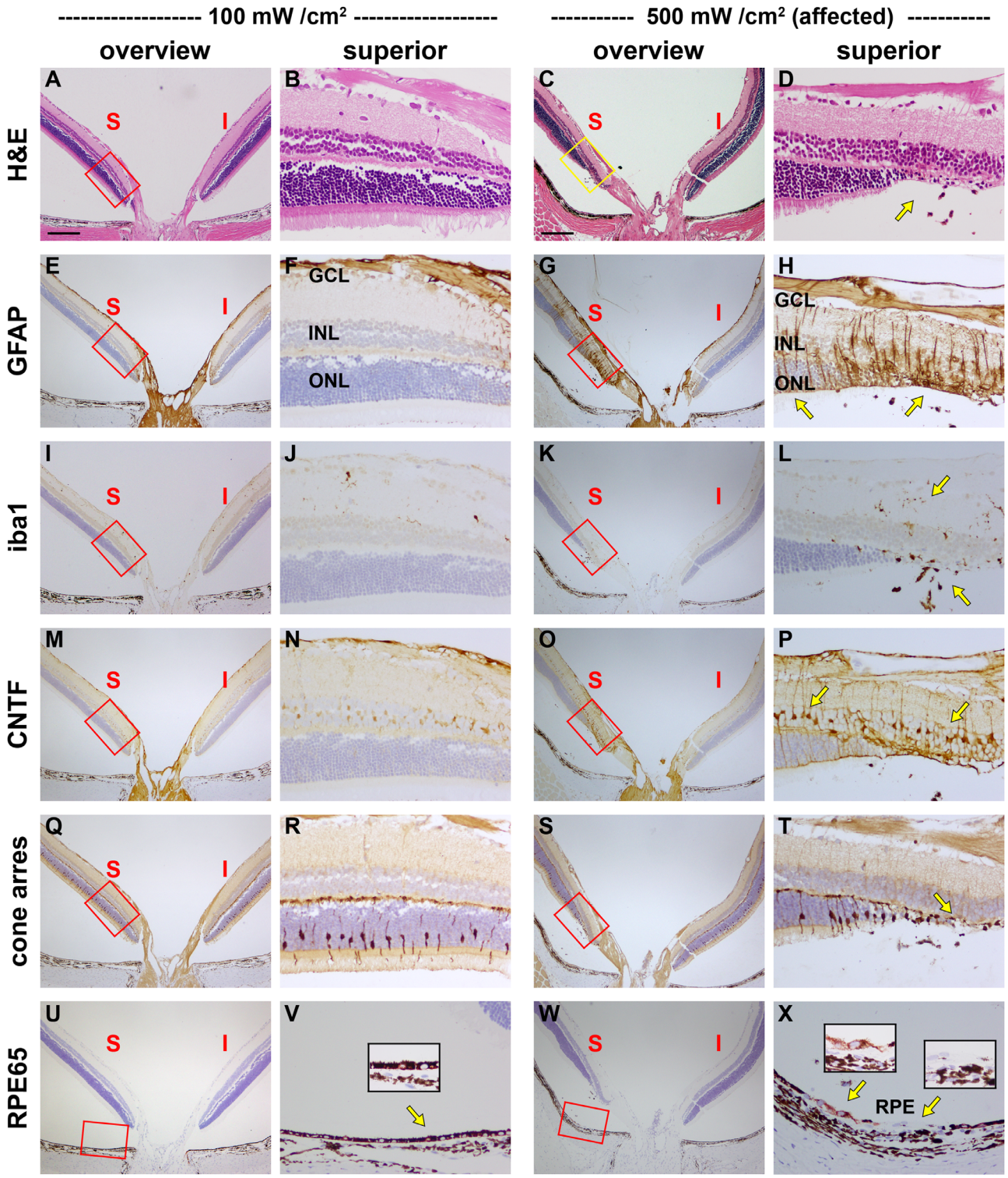

Figure 6. Effect of PBM on ONH integrity in pigmented rats at 3 days after the final treatment, as evaluated by histology and immunohistochemistry. Histology of a representative rat from the 100 mW/cm^2 group and an affected rat from the 500 mW/cm^2 group are shown. Transverse sections at the level of the ONH were stained for hematoxylin and eosin (A–D) and immunolabeled for GFAP (E–H), iba1 (I–L), CNTF (M–P), cone arrestin (cone arres, Q–T), and RPE65 (U–X). In the rat from the 100 mW/cm^2 group, there is no evidence of any histological or immunohistochemical abnormalities. In the affected rat from the 500 mW/cm^2 group, there is very localized destruction of photoreceptor rod and cone nuclei and inner and outer segments immediately superior to the ONH (C, D, S, T, arrows). This is accompanied by greatly increased expression of GFAP (G, H, arrows) and CNTF (O, P, arrows) by Müller cells and astrocytes overlying and immediately adjacent to the affected area. Numerous iba1-positive activated microglia can be observed within the damaged area of the retina (K, L, arrows). The RPE →

←
layer shows loss of RPE65 immunolabeling at the lesion (W, X, arrows, highlighted within insets). On the inferior side of the ONH, there is no patent injury or upregulation of glial markers. *Scale bar*: 250 µm (A, C, E, G, I, K, M, O, Q, S, U, W). *Scale bar*: 50 µm (B, D, F, H, J, L, N, P, R, T, V, X). GCL, ganglion cell layer; INL, inner nuclear layer.

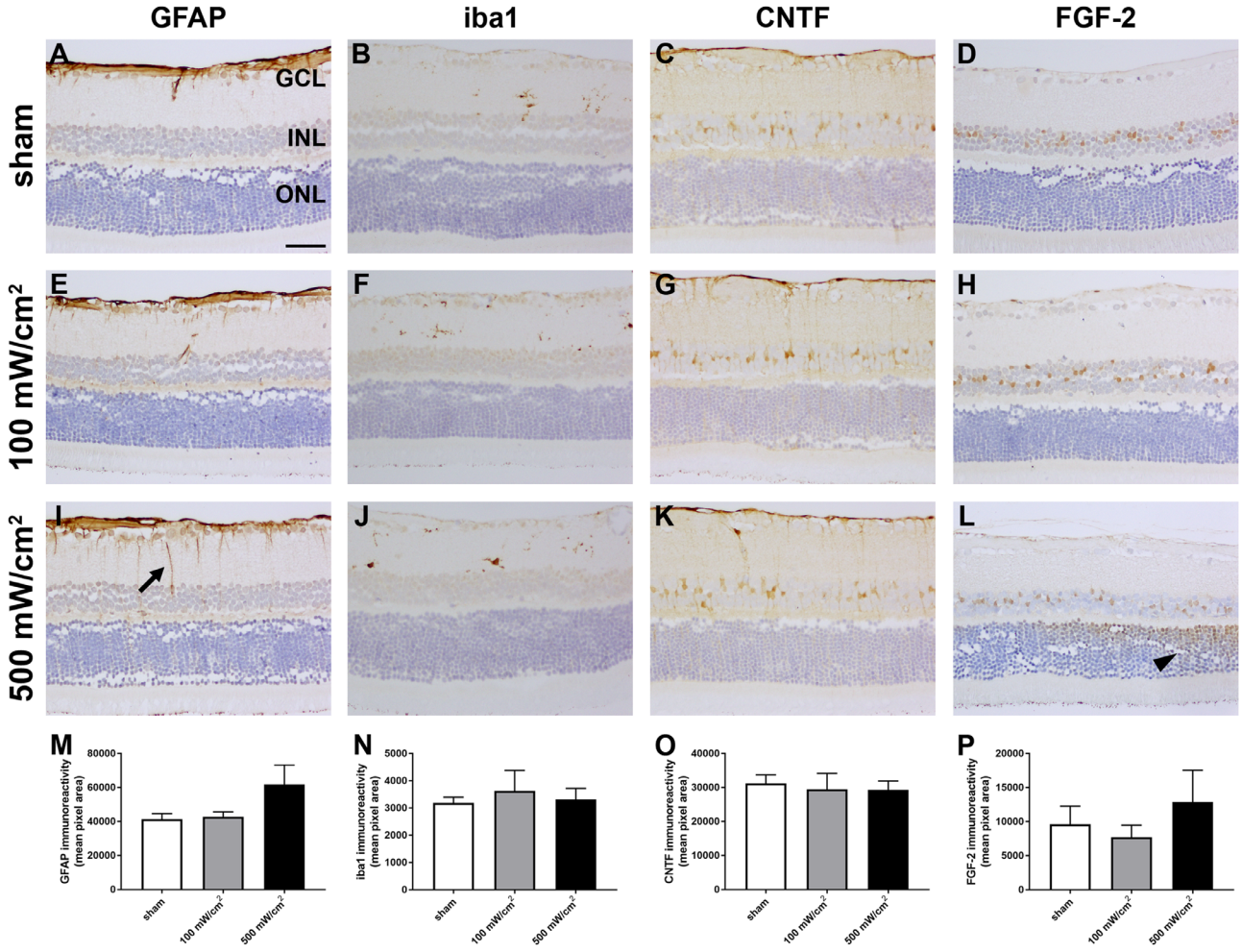

Figure 7. Effect of PBM on glial markers and stress proteins in the retina in pigmented rats at 3 days after the final treatment, as evaluated by immunohistochemistry. Representative images of retinas from sham, 100 mW/cm^2, and 500 mW/cm^2 groups immunolabeled for GFAP (A, E, I), Iba1 (B, F, J), CTNF (C, G, K), and FGF2 (D, H, L) are shown. Images were captured within the irradiated zone at approximately 1 mm from the optic nerve head. Quantification of GFAP (M), iba1 (N), CNTF (O), and FGF2 (P) abundances, as defined in the Materials and Methods section, are provided. Data are expressed as the mean ± SEM, where n = 3–6 for each group. ANOVA revealed no significant differences in GFAP, iba1, CNTF, or FGF2 abundance among treatment groups. Nevertheless, there was a tendency for elevated GFAP abundance in the 500 mW/cm^2 group (I, arrow). There was also de novo FGF2 expression by photoreceptors in one rat from the 500 mW/cm^2 group (L, arrowhead). *Scale bar*: 50 µm. GCL, ganglion cell layer; INL, inner nuclear layer.

irradiated zone (Fig. 10). Quantification of the levels of GFAP, iba1, CNTF, and FGF2 showed no statistically significant upregulations of any of these markers in the 500 mW/cm^2 group relative to the other groups ($P = 0.43$ vs. $P = 0.75$, $P = 0.71$, and $P = 0.79$, respectively, by ANOVA) (Fig. 10). Quantification of the number of RGCs in retinal tissue sections and the number of axonal cytoskeletal abnormalities in the optic nerve sections revealed no evidence of any toxicity in the PBM groups (data not shown).

Discussion

The rationale for the current study was to examine safe dosages for treatment of the retina with a novel

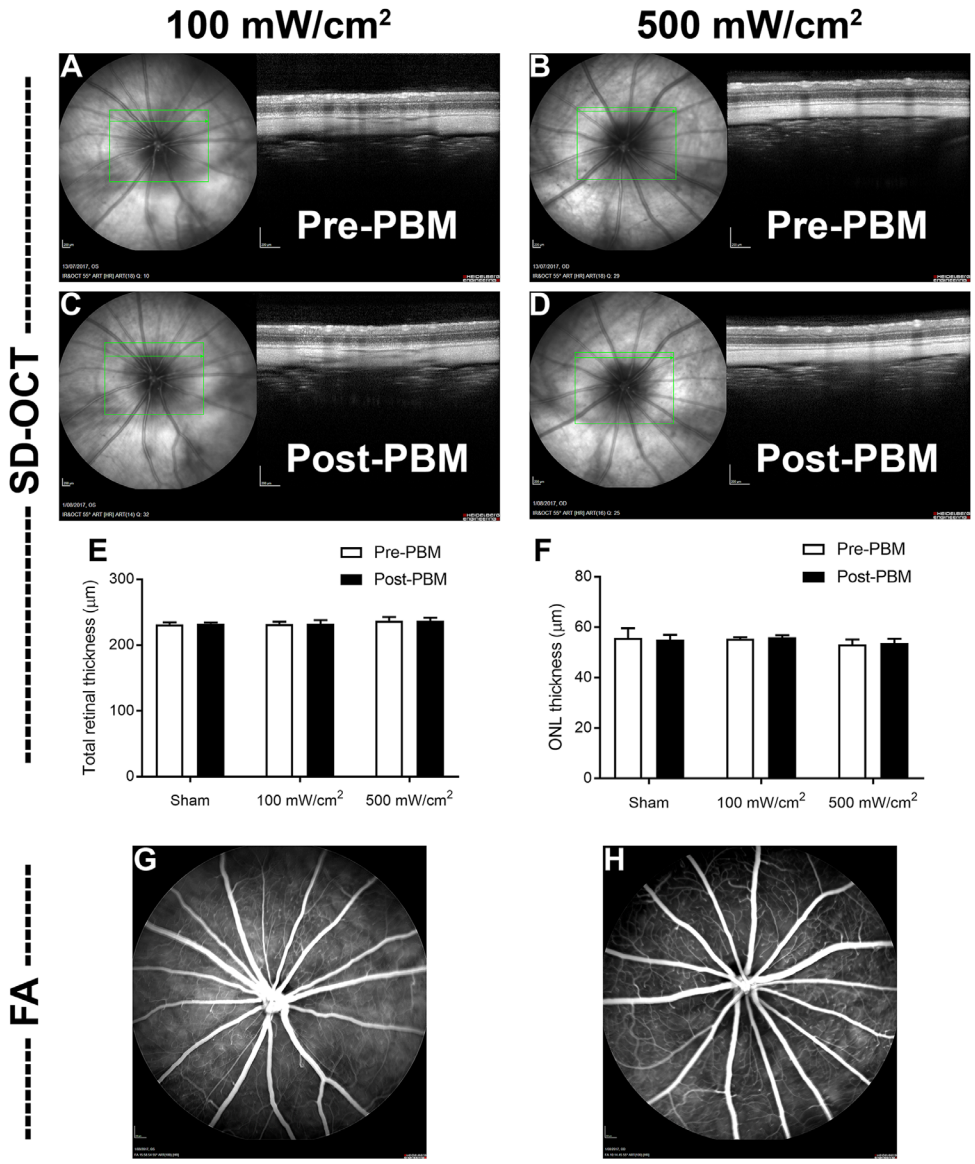

Figure 8. Effect of PBM on retinal integrity in non-pigmented rats at 1 week after the final treatment, as evaluated by fundus imaging, SD-OCT, and FA. Pre-treatment and post-treatment fundus and SD-OCT images of representative rats from 100 mW/cm^2 (A, B) and 500 mW/cm^2 groups (C, D) are shown. There are no readily discernible abnormalities in either the fundus image or SD-OCT between baseline and post-PBM at either power setting. Quantification of total retinal thickness (E) and ONL thickness (F) in the different treatment groups, as defined in the Materials and Methods section, is provided. Data are expressed as the mean ± SEM, where n = 3–6 for each group. Corresponding post-treatment FA images are shown (G, H). Images were captured 15 to 20 minutes after injection of sodium fluorescein. Images of both eyes appear normal.

PBM laser prior to preclinical assessment of neuroprotection efficacy and eventual clinical translation. There have been clinical safety studies of PBM laser for stroke[24,25] and hair loss[26] but not for treatment of retinal diseases. Safe treatment parameters from preclinical PBM studies are often difficult to extrapolate to the clinical setting due to a myriad of factors, including source of PBM, mode of delivery, wavelength of light, distance from source, and duration and energy setting of exposure, as well as physical and physiological differences among targeted tissues. The use of a slit-lamp-mounted near-infrared laser that can deliver precise doses of PBM to a defined area of the retina circumvented many of these issues, providing a foundation for future clinical testing. The overall results of this study reveal that there exists a safety threshold for laser-delivered PBM to the retina in pigmented rats—but interestingly not in non-pigmented rats—that could be identified as 500 mW/cm^2 irradiance. In non-pigmented rats, no adverse

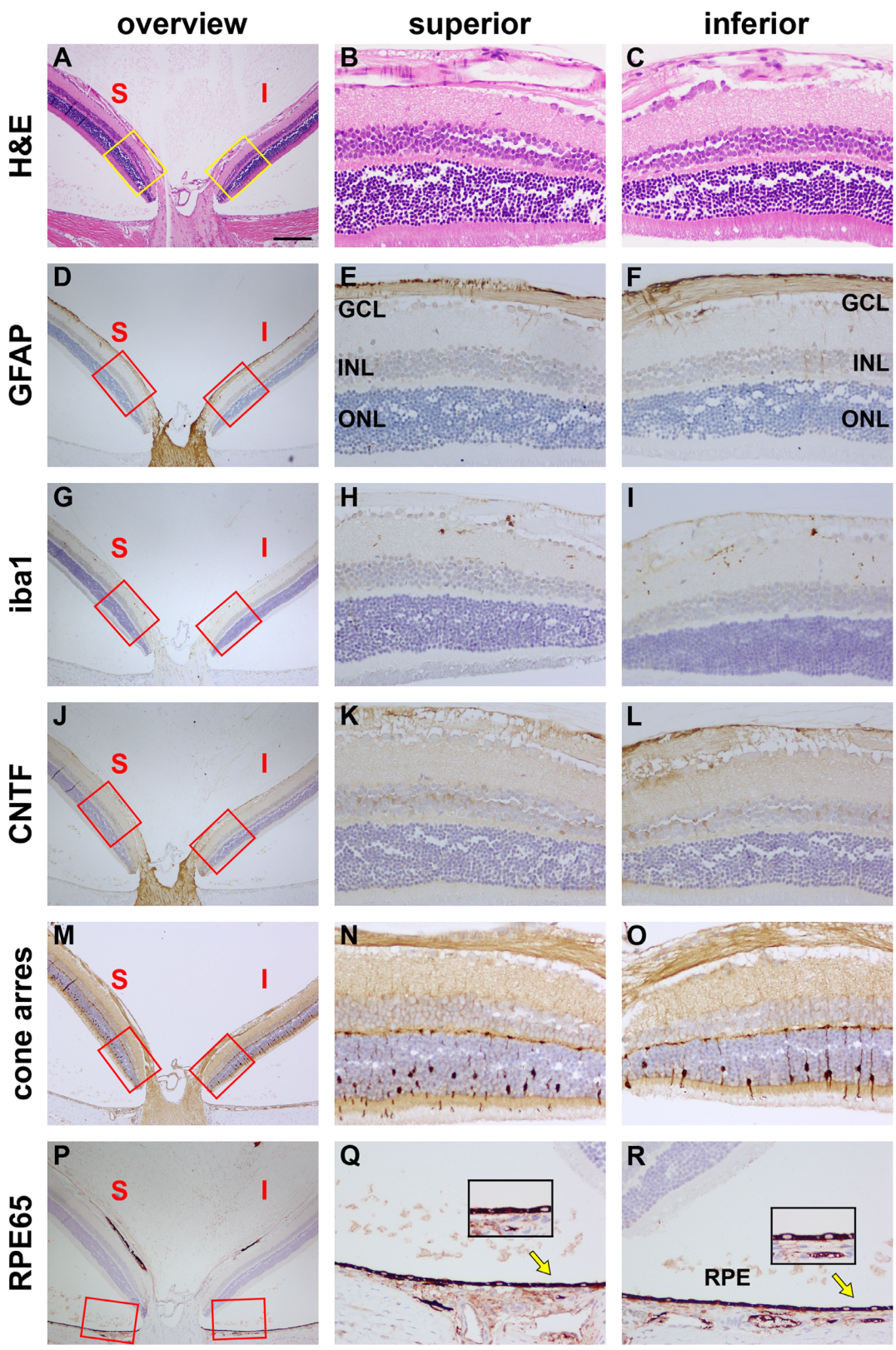

Figure 9. Effect of PBM on ONH integrity in non-pigmented rats at 1 week after the final treatment, as evaluated by histology and immunohistochemistry. Histology of a representative rat from the 500 mW/cm^2 group. Transverse sections at the level of the ONH were stained for hematoxylin and eosin (A–C) and immunolabeled for GFAP (D–F), iba1 (G–I), CNTF (J–L), cone arrestin (cone arres, M–O), and RPE65 (P–R). There is no discernible injury to rod or cone photoreceptor nuclei nor to inner and outer segments either superior or inferior to the ONH →

←

(A–C, M–O). This is no upregulation of GFAP (D–F) or CNTF (J–L) by Müller cells or astrocytes. There is no obvious increase in the number of iba1-positive microglia nor do they display any morphological signs of activation (G, H, arrows). The RPE layer appears normal on both sides of the ONH (P–R, arrows, highlighted within insets). *Scale bar*: 250 µm (A, D, G, J, M, P). *Scale bar*: 50 µm (B, C, E, F, H, I, K, L, N, O, Q, R). GCL, ganglion cell layer; INL, inner nuclear layer.

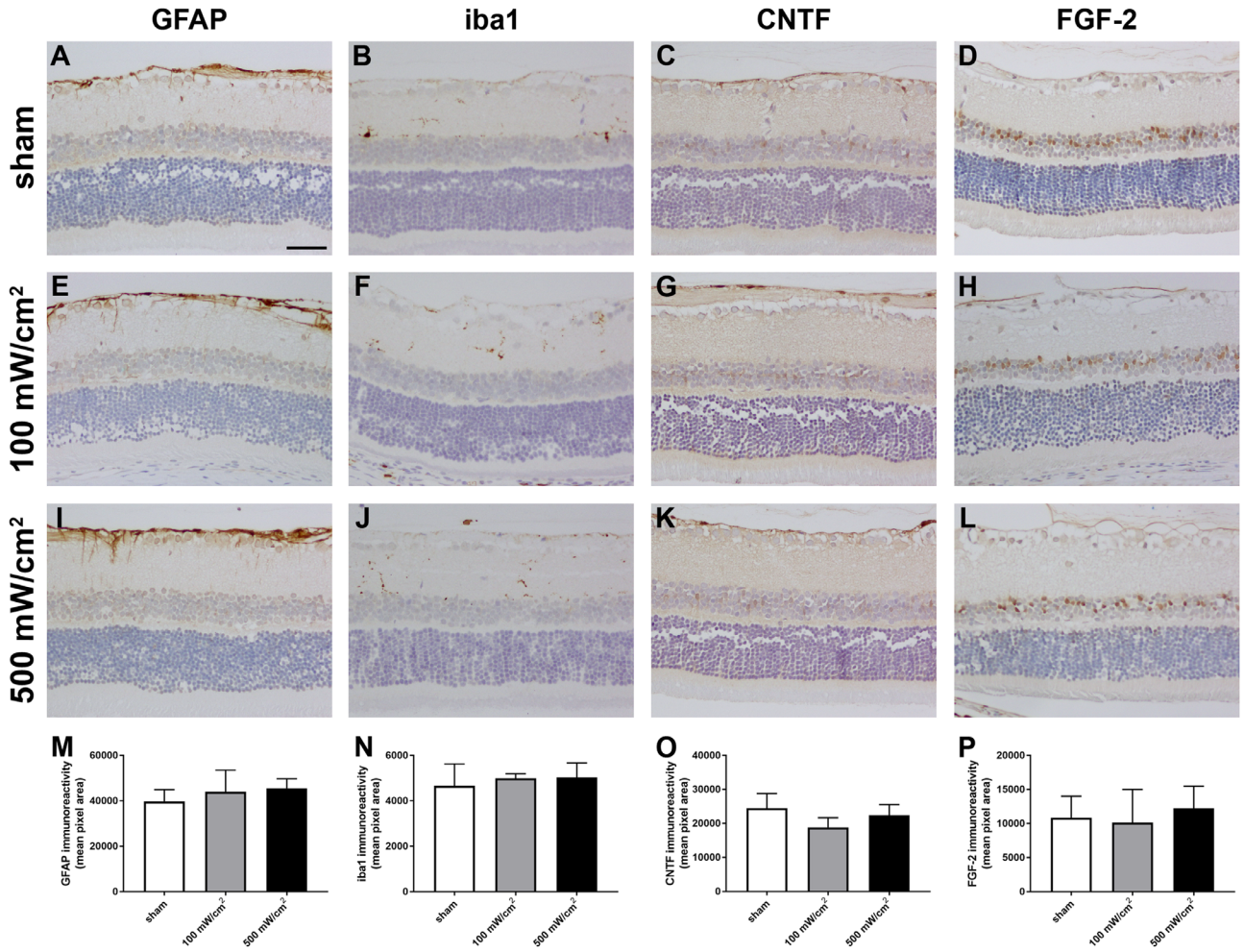

Figure 10. Effect of PBM on glial markers and stress proteins in the retina in non-pigmented rats at 1 week after the final treatment, as evaluated by immunohistochemistry. Representative images of retinas from sham, 100 mW/cm^2, and 500 mW/cm^2 groups immunolabeled for GFAP (A, E, I), Iba1 (B, F, J), CTNF (C, G, K), and FGF2 (D, H, L) are shown. Images were captured within the irradiated zone at approximately 1 mm from the optic nerve head. No discernible upregulation of any of the four markers is evident in rats treated with PBM (E–L). Quantification of GFAP (M), iba1 (N), CNTF (O), and FGF2 (P) abundances, as defined in the Materials and Methods section, are provided. Data are expressed as the mean ± SEM, where n = 3–6 for each group. ANOVA revealed no significant differences in abundances of GFAP, iba1, CNTF, or FGF2 among treatment groups. *Scale bar*: 50 µm. GCL, ganglion cell layer; INL, inner nuclear layer.

events were identified at 100 mW/cm^2 or 500 mW/cm^2 irradiances. In pigmented rats, no adverse events were identified at 25 mW/cm^2 or 100 mW/cm^2 irradiances; however, at the highest setting tested, 500 mW/cm^2, six out of 16 treated eyes displayed very localized injury in the peripapillary retina, typically immediately adjacent to the optic nerve head.

The localized damage observed in just over a third of pigmented rats treated with 500 mW/cm^2 PBM was evident in eyes analyzed at 3 days following the last laser session and in eyes assessed 1 week post-laser. SD-OCT changes corresponded well with histological assessment of the retina, which showed localized degeneration of rod and cone photoreceptor nuclei and inner and outer segments but no obvious injury to the inner layers. In the affected area of each retina, there was marked Müller cell gliosis, as revealed by increased expression of the intermediate filament GFAP and the

trophic factors CNTF and FGF2. All three proteins are reliable markers of retinal homeostatic dysfunction and injury. Upregulated GFAP is routinely considered the most sensitive and generalizable corollary of retinal injury,[27] and CNTF and FGF2 are trophic factors upregulated as part of the endogenous survival mechanism of the retina against insults as varied as light damage, trauma, ischemia, excitotoxicity, and laser injury.[28–32] In addition to Müller cell gliosis, there was also evidence of an increased presence of microglia within the affected area, presumably with the purpose of phagocytosing dying photoreceptors.

The PBM laser emits a broad, collimated beam 4.5 mm in diameter. Accordingly, the irradiated zone (approximately 16 mm^2) encompasses a considerable percentage of the rat retina, which on average equates to an area of 50 mm^2 at 2 months of age.[33] Of importance, outer retinal damage in affected eyes, whether assessed by in vivo or ex vivo means, was always restricted to the area immediately adjacent to the ONH. Moreover, upregulation of markers of gliosis/homeostatic disturbance was similarly confined to the central area of retina shown to be affected on imaging. As such, it must be concluded that there is no overt, retina-wide, homeostatic disruption resulting from PBM, even at 500 mW/cm^2 irradiance. Importantly, RGCs, which contain abundant mitochondria, notably within their unmyelinated axons within the nerve fiber layer, were not damaged at any energy setting tested.

In both cohorts of pigmented rats that received 500 mW/cm^2 (analyzed 1 week post-PBM and 3 days post-PBM), the mean reductions in total retinal thickness and ONL thickness were slight and typically did not reach significance. This outcome is not simply a reflection of the fact that only a third of eyes were affected, but also that 12 predetermined analysis points, covering an area of approximately 1 mm^2 surrounding the ONH were analyzed per eye. Due to the focal nature of the damage that occurred, the mean change in retinal thickness is not a fair indication of the pathology in the affected area. Indeed, the predetermined points may not even have captured the worst affected area. They were selected to reflect generalized changes within the irradiation zone; focal damage was not anticipated. Similar comments can be made regarding the ERG data, in which no significant changes in a- or b-wave amplitudes or implicit times were measurable. ERG is suited to detecting retina-wide visual changes, reflecting pan-retinal damage. The very focal damage observed in these rats might conceivably have been detectable on multifocal ERG.[34] Of note, scrutiny of the actual damaged area in the six affected eyes, whether by fundus imaging or SD-OCT, revealed that changes were more prominent at 1 week post-PBM than at 3 days post-laser. This conclusion is tentative due to the small number of affected eyes. Nevertheless, if accurate, it suggests an evolving dysfunction and/or loss of photoreceptors in the affected area. Expansion of the lesion is a well-described phenomenon in rodent[35,36] and human[37,38] retinas in the early period following laser photocoagulation that is attributed to secondary degeneration of photoreceptors. It is possible that a similar response can occur following exposure to very high-dose PBM.

Of the six pigmented rats treated with 500 mW/cm^2 that exhibited focal retinal damage, only two demonstrated overt FA changes, both in the cohort analyzed 1 week post-PBM. The FA change was manifest as a hyperfluorescent area that remained uniform in size throughout the angiogram. We have interpreted this finding as an RPE "window defect" indicative of loss of RPE,[39] a finding given support by the histopathology data. Nevertheless, we must be mindful that fluorescein was administered intraperitoneally in rats; thus, the kinetics of rodent FA cannot be directly correlated with clinical angiograms. It is unclear why only two rats demonstrated this pathological feature despite all six displaying outer retinal damage. The logical deduction is that the FA findings correlated with the extent of RPE damage in each rat.

The explanation for the localized damage seen following high dose PBM is presently unknown. Potential mechanisms of laser-induced damage include photochemical, photomechanical and photothermal reactions.[40] Photomechanical damage occurs due to mechanical compressive or tensile forces (shock waves) resulting from rapid absorption of high irradiance energy into RPE melanosomes.[41] Photomechanical damage is extremely unlikely to underlie the retinal damage observed following laser-delivered PBM given that it requires enormous irradiance doses (megawatts or terawatts per square centimeter) coupled with extremely brief exposure times in the range of nanoseconds to picoseconds.

Photochemical damage is non-thermal, non-mechanical damage that is hypothesized to be caused by reactive oxygen species and other free radicals that are generated following interaction of irradiation from high-energy visible light with chromophore molecules contained within the retina and RPE.[40,42] Because photochemical damage occurs following exposure to natural light, it has been widely studied in recent decades. Photochemical damage can be categorized into class I and class II types. The former is believed to be mediated by interaction with visual pigments, with the primary lesion being located in the photoreceptors. Class I damage typically occurs after long

exposure to low irradiances of white light. Class II damage displays an action spectrum that peaks at shorter wavelength light, chiefly ultraviolet to blue light, and occurs following exposure to higher irradiances of light, with the primary lesion being located in the RPE. The mechanisms underlying photochemical damage have not been unequivocally identified but are thought to involve lipid and protein peroxidation of the neurosensory retina and RPE.[40,42] Given that the PBM laser emits long-wavelength light of 670 nm, that total exposure was restricted to three sessions of 90 seconds, and that albino eyes were unaffected, a photochemical cause might appear unlikely. Nevertheless, varying the duration and the number of sessions in future studies may provide evidence as to whether a photochemical component is present.

Photothermal damage derives from photon absorption by tissue molecules causing an increased mean kinetic energy, which is dissipated by molecules colliding, thereby resulting in a temperature rise.[40] Generally, red light and near-infrared light are associated with photothermal injury. Permanent thermal damage typically occurs when the temperature in the target area rises by a minimum of 10°C. Photon absorption is facilitated by pigments, including melanin, which is most abundant in the RPE and choroid. Pigmented strains necessarily have melanin in their RPE/choroid and hence are far more susceptible to photothermal laser damage than albino rats. Moreover, photothermal damage to the retina is concentrated in the cell layer adjacent to the RPE, the ONL,[43–46] which is consistent with the findings of this study. The current findings bear cursory similarity to those of a safety study of transcranial, laser-delivered, 808-nm PBM in rat brain, which reported no effects at doses up to 375 mW/cm^2 irradiance; however, rats treated with 750 mW/cm^2 irradiance exhibited features consistent with photothermal damage.[47] These rats displayed heat-related skin reddening and blistering in irradiated areas, and histological analysis of affected brain tissue revealed focal areas characterized by subdural necrosis, loss of neuronal tissue, infiltration of macrophages, and meningeal artery degeneration.

Of the various theoretical possibilities, photothermal damage would seem to be the most likely mechanism underlying the observed PBM-induced injury, due to the restricted damage profile across the retinal layers and the fact that only pigmented rats were affected; however, this is only a partially satisfactory explanation, as the PBM laser has a flat-top beam profile and thus broader damage would have been expected across the entire irradiance zone. It is, of course, possible that the damage profile observed is specific to the heavily pigmented, inbred Dark Agouti rat strain and the results are not generalizable to all pigmented eyes. Further testing might be warranted in a different pigmented strain. Furthermore, it should be noted that this study has investigated retinal changes in the acute phase after laser application. Conceivably, subtle retinal pathology could develop at longer time points, and the pathology that was noted may not be static; for example, the laser-induced lesion may enlarge over time. These caveats are important, and we should remain mindful of possible long-term adverse effects of this laser and any new therapeutic modality.

Acknowledgments

The authors are grateful to Mark Daymon and Sergi Kozirev for expert technical assistance.

Supported by the Ophthalmic Research Institute of Australia and by an Innovation Connections grant from the Federal Government of Australia. The funding source had no role in the design and conduct of the study; collection, management, analysis, and interpretation of the data; preparation, review, or approval of the manuscript; or decision to submit the manuscript for publication.

Disclosure: **J. Ao**, None; **G. Chidlow**, None; **J.P.M. Wood**, None; **R.J. Casson**, None

References

1. Mester E, Spiry T, Szende B, Tota JG. Effect of laser rays on wound healing. *Am J Surg*. 1971;122:532–535.
2. Chung H, Dai T, Sharma SK, Huang YY, Carroll JD, Hamblin MR. The nuts and bolts of low-level laser (light) therapy. *Ann Biomed Eng*. 2012;40:516–533.
3. Karu TI. Cellular and molecular mechanisms of photobiomodulation (low-power laser therapy). *IEEE J Sel Top Quantum Electron*. 2014;20:7000306–7000306.
4. Marcus RA, Sutin N. Electron transfer in chemistry and biology. *Biochem Biophys Acta*. 1985;811:265–322.
5. Eells JT, Henry MM, Summerfelt P, et al. Therapeutic photobiomodulation for methanol-induced retinal toxicity. *Proc Natl Acad Sci USA*. 2003;100:3439–3444.
6. Albarracin R, Eells J, Valter K. Photobiomodulation protects the retina from light-induced

photoreceptor degeneration. *Invest Ophthalmol Vis Sci*. 2011;52:3582–3592.
7. Albarracin R, Valter K. 670 nm red light preconditioning supports Müller cell function: evidence from the white light-induced damage model in the rat retina. *Photochem Photobiol*. 2012;88:1418–1427.
8. Albarracin RS, Valter K. Treatment with 670-nm light protects the cone photoreceptors from white light-induced degeneration. *Adv Exp Med Biol*. 2012;723:121–128.
9. Natoli R, Zhu Y, Valter K, Bisti S, Eells J, Stone J. Gene and noncoding RNA regulation underlying photoreceptor protection: microarray study of dietary antioxidant saffron and photobiomodulation in rat retina. *Mol Vis*. 2010;16:1801–1822.
10. Qu C, Cao W, Fan Y, Lin Y. Near-infrared light protect the photoreceptor from light-induced damage in rats. *Adv Exp Med Biol*. 2010;664:365–374.
11. Di Marco F, Di Paolo M, Romeo S, et al. Combining neuroprotectants in a model of retinal degeneration: no additive benefit. *PLoS One*. 2014;9:e100389.
12. Giacci MK, Wheeler L, Lovett S, et al. Differential effects of 670 and 830 nm red near infrared irradiation therapy: a comparative study of optic nerve injury, retinal degeneration, traumatic brain and spinal cord injury. *PLoS One*. 2014;9:e104565.
13. Albarracin R, Natoli R, Rutar M, Valter K, Provis J. 670 nm light mitigates oxygen-induced degeneration in C57BL/6J mouse retina. *BMC Neurosci*. 2013;14:125.
14. Natoli R, Valter K, Barbosa M, et al. 670nm photobiomodulation as a novel protection against retinopathy of prematurity: evidence from oxygen induced retinopathy models. *PLoS One*. 2013;8:e72135.
15. Cheng Y, Du Y, Liu H, Tang J, Veenstra A, Kern TS. Photobiomodulation inhibits long-term structural and functional lesions of diabetic retinopathy. *Diabetes*. 2018;67:291–298.
16. Tang J, Herda AA, Kern TS. Photobiomodulation in the treatment of patients with non-center-involving diabetic macular oedema. *Br J Ophthalmol*. 2014;98:1013–1015.
17. Merry GF, Munk MR, Dotson RS, Walker MG, Devenyi RG. Photobiomodulation reduces drusen volume and improves visual acuity and contrast sensitivity in dry age-related macular degeneration. *Acta Ophthalmol*. 2017;95:e270–e277.
18. Fitzgerald M, Hodgetts S, Van Den Heuvel C, et al. Red/near-infrared irradiation therapy for treatment of central nervous system injuries and disorders. *Rev Neurosci*. 2013;24:205–226.
19. Ao JZJ, Chidlow G, Wood JPM, Casson RJ. Evaluation of the safety of laser-delivered Photobiomodulation and its neuroprotection efficacy in a mouse model of Retinitis Pigmentosa. *Invest Ophthalmol Vis Sci*. 2018;59:961.
20. Bawa G, Tkatchenko TV, Avrutsky I, Tkatchenko AV. Variational analysis of the mouse and rat eye optical parameters. *Biomed Opt Express*. 2013;4:2585–2595.
21. Chidlow G, Daymon M, Wood JP, Casson RJ. Localization of a wide-ranging panel of antigens in the rat retina by immunohistochemistry: comparison of Davidson's solution and formalin as fixatives. *J Histochem Cytochem*. 2011;59:884–898.
22. Chidlow G, Wood JP, Knoops B, Casson RJ. Expression and distribution of peroxiredoxins in the retina and optic nerve. *Brain Struct Funct*. 2016;221:3903–3925.
23. Chidlow G, Ebneter A, Wood JP, Casson RJ. The optic nerve head is the site of axonal transport disruption, axonal cytoskeleton damage and putative axonal regeneration failure in a rat model of glaucoma. *Acta Neuropathol*. 2011;121:737–751.
24. Lampl Y, Zivin JA, Fisher M, et al. Infrared laser therapy for ischemic stroke: a new treatment strategy: results of the NeuroThera Effectiveness and Safety Trial-1 (NEST-1). *Stroke*. 2007;38:1843–1849.
25. Zivin JA, Albers GW, Bornstein N, et al. Effectiveness and safety of transcranial laser therapy for acute ischemic stroke. *Stroke*. 2009;40:1359–1364.
26. Jimenez JJ, Wikramanayake TC, Bergfeld W, et al. Efficacy and safety of a low-level laser device in the treatment of male and female pattern hair loss: a multicenter, randomized, sham device-controlled, double-blind study. *Am J Clin Dermatol*. 2014;15:115–127.
27. Bringmann A, Pannicke T, Grosche J, et al. Müller cells in the healthy and diseased retina. *Prog Retin Eye Res*. 2006;25:397–424.
28. Wen R, Cheng T, Song Y, et al. Continuous exposure to bright light upregulates bFGF and CNTF expression in the rat retina. *Curr Eye Res*. 1998;17:494–500.
29. Wen R, Song Y, Cheng T, et al. Injury-induced upregulation of bFGF and CNTF mRNAS in the rat retina. *J Neurosci*. 1995;15:7377–7385.
30. Ju W-K, Lee M-Y, Hofmann H-D, Kirsch M, Chun M-H. Expression of CNTF in Müller cells of the rat retina after pressure-induced ischemia. *Neuroreport*. 1999;10:419–422.
31. Honjo M, Tanihara H, Kido N, Inatani M, Okazaki K, Honda Y. Expression of ciliary neurotrophic factor activated by retinal Müller

cells in eyes with NMDA- and kainic acid-induced neuronal death. *Invest Ophthalmol Vis Sci*. 2000;41:552–560.
32. Chidlow G, Daymon M, Wood JP, Casson RJ. Localization of a wide-ranging panel of antigens in the rat retina by immunohistochemistry: comparison of Davidson's solution and formalin as fixatives. *J Histochem Cytochem*. 2011;59:884–898.
33. Nadal-Nicolas FM, Vidal-Sanz M, Agudo-Barriuso M. The aging rat retina: from function to anatomy. *Neurobiol Aging*. 2018;61:146–168.
34. Azarmina M. Full-field versus multifocal electroretinography. *J Ophthalmic Vis Res*. 2013;8:191–192.
35. Belokopytov M, Belkin M, Dubinsky G, Epstein Y, Rosner M. Development and recovery of laser-induced retinal lesion in rats. *Retina*. 2010;30:662–670.
36. Rosner M, Solberg Y, Turetz J, Belkin M. Neuroprotective therapy for argon-laser induced retinal injury. *Exp Eye Res*. 1997;65:485–495.
37. Schatz H, Madeira D, McDonald HR, Johnson RN. Progressive enlargement of laser scars following grid laser photocoagulation for diffuse diabetic macular edema. *Arch Ophthalmol*. 1991;109:1549–1551.
38. Maeshima K, Utsugi-Sutoh N, Otani T, Kishi S. Progressive enlargement of scattered photocoagulation scars in diabetic retinopathy. *Retina*. 2004;24:507–511.
39. Krill AE, Newell FW, Chishti MI. Fluorescein studies in diseases affecting the retinal pigment epithelium. *Am J Ophthalmol*. 1968;66:470–484.
40. Youssef PN, Sheibani N, Albert DM. Retinal light toxicity. *Eye (Lond)*. 2011;25:1–14.
41. Jacques SL. Laser-tissue interactions. Photochemical, photothermal, and photomechanical. *Surg Clin North Am*. 1992;72:531–558.
42. Wu J, Seregard S, Algvere PV. Photochemical damage of the retina. *Surv Ophthalmol*. 2006;51:461–481.
43. van Norren D, Vos JJ. Light damage to the retina: an historical approach. *Eye (Lond)*. 2016;30:169–172.
44. Brancato R, Pratesi R, Leoni G, Trabucchi G, Vanni U. Histopathology of diode and argon laser lesions in rabbit retina. A comparative study. *Invest Ophthalmol Vis Sci*. 1989;30:1504–1510.
45. Green WR, Robertson DM. Pathologic findings of photic retinopathy in the human eye. *Am J Ophthalmol*. 1991;112:520–527.
46. Youssef P, Sheibani N, Albert D. Retinal light toxicity. *Eye*. 2011;25:1.
47. Ilic S, Leichliter S, Streeter J, Oron A, DeTaboada L, Oron U. Effects of power densities, continuous and pulse frequencies, and number of sessions of low-level laser therapy on intact rat brain. *Photomed Laser Surg*. 2006;24:458–466.